Title: Bacterial sepsis triggers stronger transcriptomic responses in larger primates

Authors: Ryan McMinds[1,2]*, Rays H.Y. Jiang[1,2], Swamy R. Adapa[1,2], Emily Cornelius Ruhs[1,3,4], Rachel A. Munds[1], Jennifer W. Leiding[5,6], Cynthia J. Downs[7]†, Lynn B. Martin[1]†*

Affiliations:
[1]Center for Global Health and Infectious Diseases Research (GHIDR), University of South Florida; Tampa, Florida, USA
[2]USF Genomics program, University of South Florida College of Public Health, Tampa, Florida USA
[3]Department of Ecology and Evolution, University of Chicago; Chicago, Illinois, USA
[4]Grainger Center for Bioinformatics, Field Museum of Natural History; Chicago, IL.
[5]Division of Allergy and Immunology, Department of Pediatrics, Johns Hopkins University, Baltimore, FL
[6]Institute for Clinical and Translational Research, Johns Hopkins All Children's Hospital, St. Petersburg, FL
[7]Department of Environmental Biology, SUNY College of Environmental Science and Forestry; Syracuse, New York, USA
†Shared senior authorship
*Corresponding authors. Emails: r.mcminds@gmail.com, lbmartin@usf.edu

Abstract: Empirical data relating body mass to defense against infections remain limited. Recent studies have led to the Safety Factor hypothesis, which proposes that larger organisms must evolve stronger immune defenses because they carry greater risks of exposure to pathogens and parasites. Using RNAseq on blood from nine primate species exposed to bacterial lipopolysaccharides, we fit phylogenetic models and discovered hypermetric scaling in innate immune gene responses. We speculate that immune allometries may lead to asymmetrical expectations for virulence of zoonotic pathogens, such that diseases originating in smaller species may cause more severe immunopathology in larger species. This study contributes to the growing body of research on immune allometry, highlighting its importance in understanding the complex interplay between body size and immunity over evolutionary timescales.

One Sentence Summary: Immune genes are expressed disproportionately more in large than small primate species in response to simulated infection.

Introduction:

The body size of organisms profoundly affects most of their life processes (*1*). Partly, these effects are due to physical forces affecting how materials are moved into and out of cells, but evolutionary factors, too, can influence how size affects life (*2*). For instance, reaching a large size inherently requires time, so selection should act strongly on developmental rates and age-

specific breeding traits, which could lead to innovative molecular or physiological mechanisms that circumvent some physical constraints. Relationships between size and biological traits are often modeled as trait ~ $\alpha * mass^{\beta}$, which can be linearized via log-transformation of both body mass and the response variable (i.e., log(trait) ~ log(α) + β * log(mass)). Relationships between body mass and response variables are then represented by the slope coefficients, β, which can be estimated with linear regression. Traits such as blood volume and length of the digestive tract scale proportionally to body size (i.e., isometrically), with β approximately equal to 1. Other traits, such as hematocrit, also scale isometrically (*3*, *4*), but because they are independent of body mass, they have coefficients approximately equal to 0. Allometric relationships, where β deviates from the proportional expectation, are also quite common. A trait with β greater than isometry is called hypermetric whereas one with β less than isometry is hypometric. A prime example of hypoallometry is metabolic rate, which scales at ¾ the rate of body mass change at the organismal level, or equivalently, has β = -¼ when normalized to body mass (*5*–*7*).

Biological scaling has been investigated extensively. Metabolic allometries have been so powerful as to lead to the Metabolic Theory of Ecology (MTE) (*5*, *8*). Although contentious (*9*–*12*), this concept has been useful for everything from improving the conservation of wildlife to understanding the structure of human cities (*1*). Nevertheless, the MTE so far appears to hold little utility for understanding how defenses, specifically immune system processes, relate to body size. Whereas the MTE predicts hypometric immune cell concentrations ($\beta \approx$ -¼) (*13*), granulocyte concentrations in birds and mammals in fact scale hypermetrically (heterophils and neutrophils scale with β = 0.19 and 0.11, respectively) (*14*, *15*). These unexpected results suggest that other processes must come into play to explain how defenses scale with body size, and the Safety Factor hypothesis was recently offered as an eco-evolutionary explanation (*16*). This hypothesis proposes that large organisms are exposed to more and more diverse pathogens within and between generations, such that the risks and consequences of infection are much higher compared to smaller species. As a result, large species may be selected to evolve exceptionally strong defenses compared to small species (*15*).

Much like cell concentrations, gene expression (i.e., the concentration of gene transcripts) is predicted by the MTE to scale hypometrically, and a recent study provides evidence that this is broadly true across the transcriptome (*17*). However, whether immune genes are an exception to this trend is unknown. Immune gene expression is of particular interest because it could give more insight into the granulocyte hyperallometry previously described. Moreover, hypermetric immune gene expression could provide large species with disproportionately stronger defenses, represent a greater relative investment of resources towards immune gene expression compared to other genes, or be a mechanism to mitigate per-cell deficiencies in the synthesis of defensive products given declining cellular metabolic rates with increasing size. Other recent studies produced data consistent with immune gene hyperallometry, but due to their limited

phylogenetic sampling, they could not disambiguate allometric effects from effects of shared ancestry or other confounding variables (*18*, *19*).

In principle, the prediction for exceptionally strong defenses in large species could be fulfilled by hypermetric baseline expression (i.e., the immune system maintains *consistently* high constitutive expression of defensive genes), by hypermetric response to infection (i.e., immune gene expression is *increased only after detection* of a pathogen), or by both. In plants, long-lived and large species tend to invest more in constitutive barriers than in responses to invading pathogens (*20*). Similar patterns have also been suggested across vertebrates (*21*, *22*), and such a strategy could be necessary in the context of the slower metabolism observed in larger animals. However, higher baseline gene expression would be more costly, and the balance of these tradeoffs is unclear. Thus, in exploring the allometry of immune gene expression, we designed our study to be able to distinguish among the allometry of baseline (constitutive) expression, allometry of total expression during sepsis, and allometry of the response to infection (i.e., the change in gene expression between baseline and sepsis; Fig. 1).

To do this, we compared the transcriptomic profiles of replicate aliquots of live blood from nine primate species after i) a standard dose of lipopolysaccharide (LPS) from *Escherichia coli* to simulate sepsis, and ii) a null treatment of LPS-free growth media to assess baseline expression. Unlike a recent similar study (*18*), which included only four relatively large catarrhine species, our study included platyrrhine and strepsirrhine species as well, and spanned almost the full range of body masses of species in the Primates order (Fig. 2). We used phylogenetic generalized linear mixed models (pGLMMs) to link raw count data of each gene with fixed effects of the form $\alpha + \beta_1 * \text{treatment} + \beta_2 * \log(\text{mass}) + \beta_3 * \text{treatment} * \log(\text{mass})$ (Fig. 1). Models also included an offset to compensate for transcript compositionality, additional fixed effects to control for within-species differences in body size, and random effects to control for shared phylogenetic history, repeated measures, and statistical overdispersion. By standardizing our simulated sepsis methods and comparing transcriptomic responses in a phylogenetically informed context, we revealed that innate immune gene expression in response to simulated sepsis scales hypermetrically among Primates.

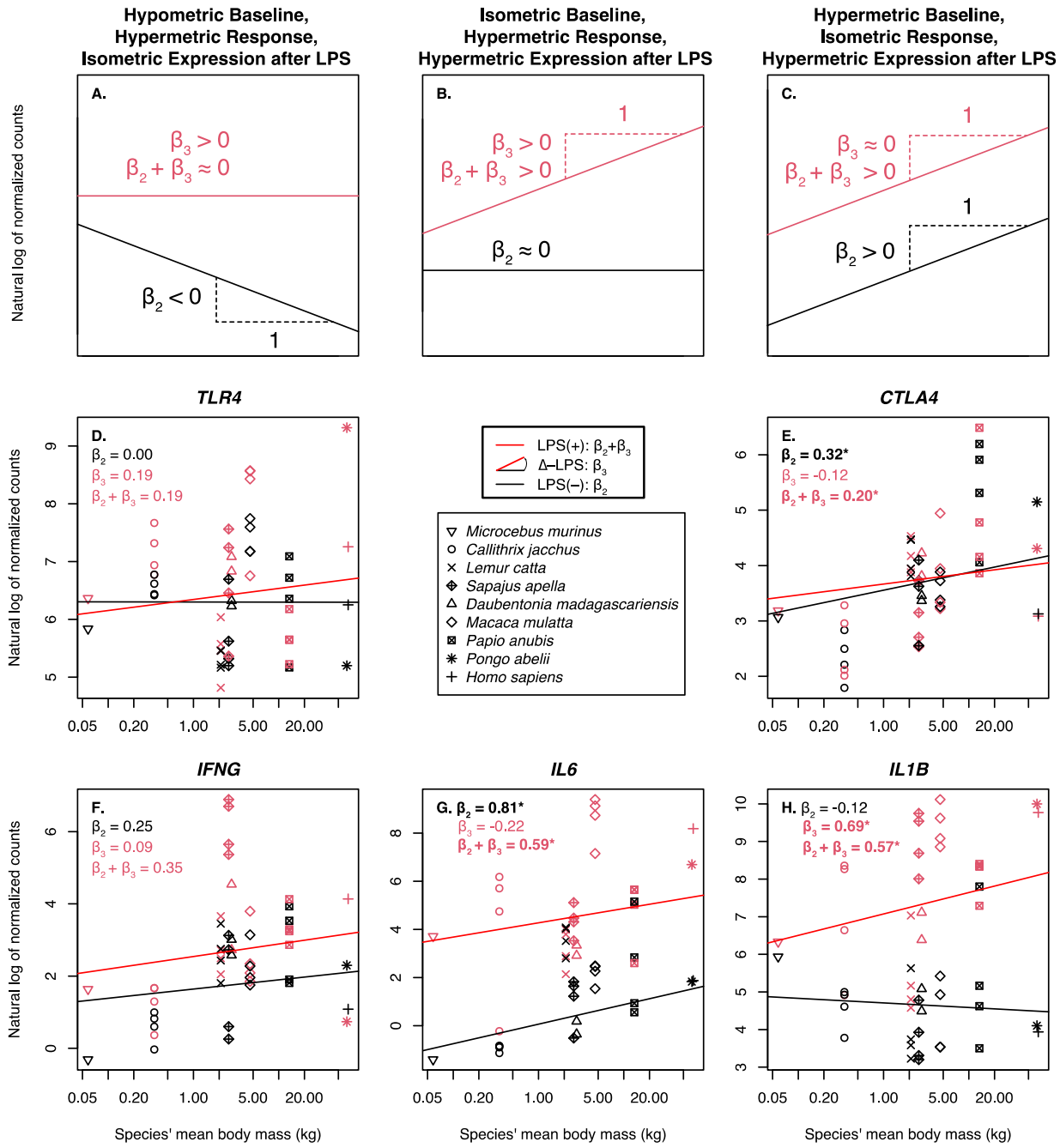

Fig. 1. Immune genes are characterized by distinct allometries that often result in hypermetric expression during simulated sepsis. (**A-C**) Example expression patterns demonstrate how phylogenetic generalized linear mixed model (pGLMM) coefficients correspond to different forms of allometry. (**A**) Hypometric baseline expression ($\beta_2 < 0$) is compensated for with a hypermetric response to LPS ($\beta_3 > 0$), resulting in isometric total expression during infection ($\beta_2 + \beta_3 \sim 0$). (**B**) Isometric baseline expression ($\beta_2 \sim 0$) plus a hypermetric response to LPS ($\beta_3 > 0$) results in hypermetric total expression during infection ($\beta_2 + \beta_3 > 0$). (**C**) Hypermetric baseline expression ($\beta_2 > 0$) plus an isometric response to LPS ($\beta_3 \sim 0$) results in hypermetric total expression during infection ($\beta_2 + \beta_3 > 0$). Note that intercepts (α and $\alpha + \beta_1$) are ignored in the discussion of these allometric patterns. (**D-H**) Log abundance (relative to the per-sample size factor and after adding a pseudocount of 0.5) of five example genes (HGNC gene names *TLR4*, *CTLA4*, *IFNG*, *IL6*, and *IL1B*, respectively) as a function of species' average body

mass in kilograms (plotted on log scale). Symbols correspond to species (▽= *Microcebus murinus*, ○ = *Callithrix jacchus*, × = *Lemur catta*, ◇+ = *Sapajus apella*, △ = *Daubentonia madagascariensis*, ◇ = *Macaca mulatta*, ⊠ = *Papio anubis*, ∗ = *Pongo abelii*, + = *Homo sapiens*). Black points correspond to samples with control treatment, and red points correspond to samples with LPS treatment. Fitted lines are plotted using coefficients extracted from the pGLMMs. pGLMM coefficients are listed, with an asterisk (*) if the 95% credible interval did not include zero.

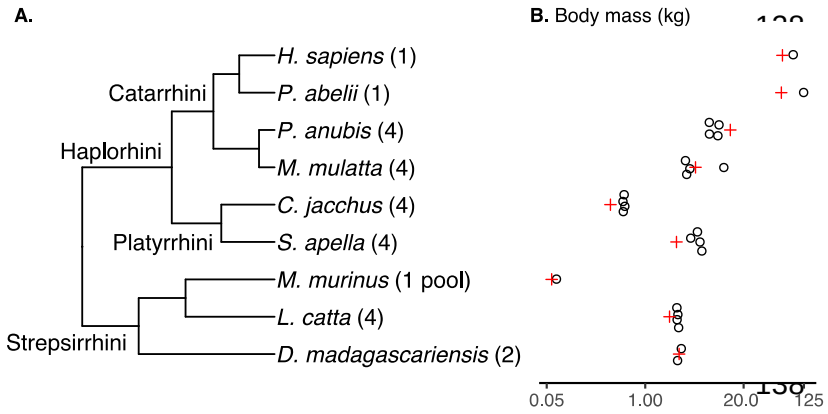

Fig. 2. Body mass and phylogenetic relationships among samples. (**A**) Primates phylogeny derived from (*23*). Tips are annotated with the numbers of individuals sampled for the present study (the pool for *M. murinus* consisted of 8 individuals). (**B**) Body mass (kg) in the context of their phylogenetic relationships (° = individuals in our study, + = species mean from (*24*).

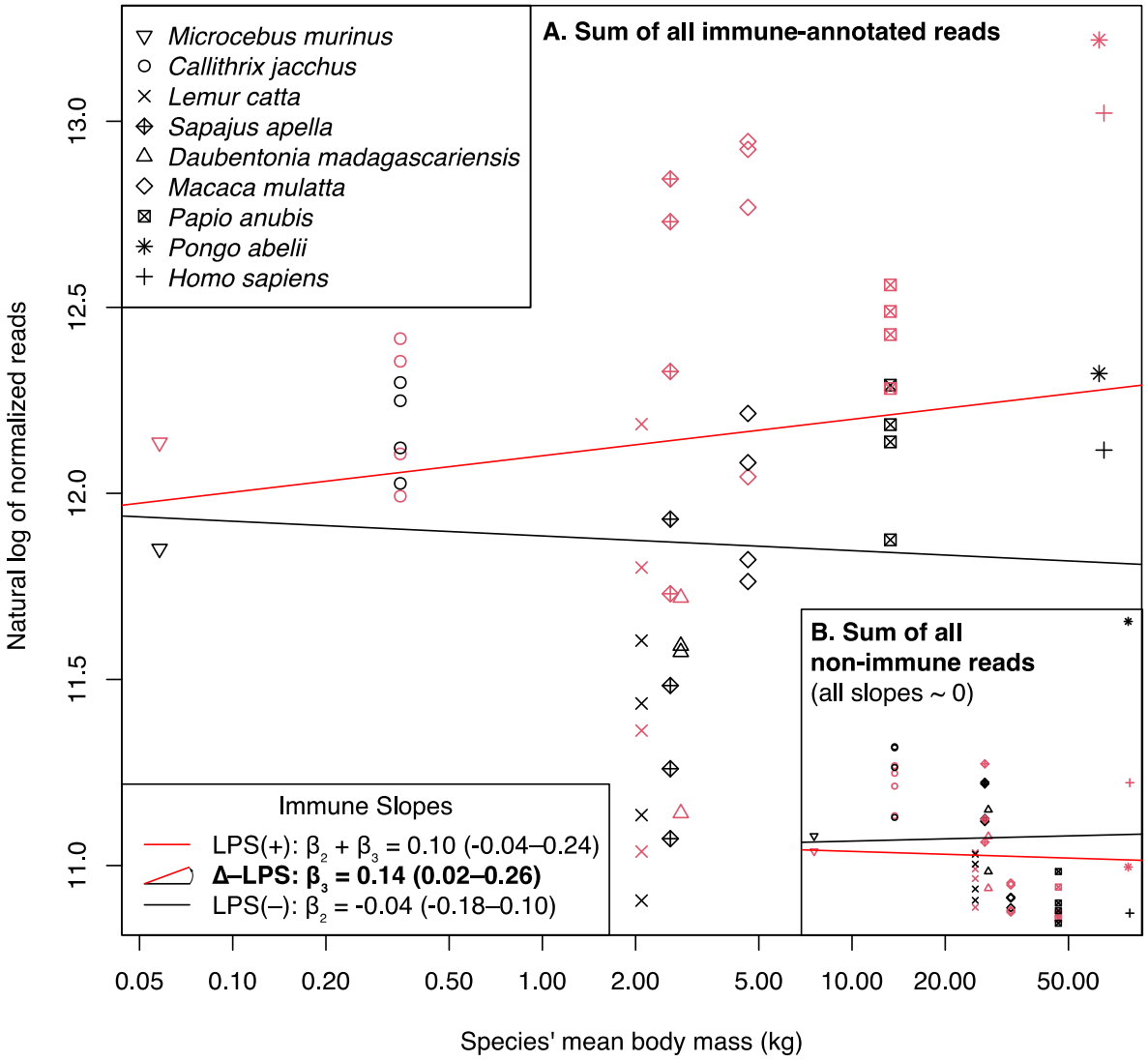

Fig. 3. Change in total immune gene expression scales hypermetrically in response to simulated sepsis among nine primate species. (**A**) Log abundance (relative to the per-sample size factor and after adding a pseudocount of 0.5) of all reads belonging to immune-annotated 1:1 orthologous genes as a function of species' average body mass in kilograms (plotted on log scale). Symbols correspond to species (▽= *Microcebus murinus*, ○ = *Callithrix jacchus*, × = *Lemur catta*, ◇+ = *Sapajus apella*, △ = *Daubentonia madagascariensis*, ◇ = *Macaca mulatta*, ⊠ = *Papio anubis*, ∗ = *Pongo abelii*, + = *Homo sapiens*). Black points correspond to samples with control treatment, and red points to samples with LPS treatment. Fitted lines are plotted using coefficients extracted from the pGLMMs. pGLMM coefficients are listed in the lower left legend, with the estimate followed by the 95% credible interval. (**B**) Log relative abundance of non-immune-annotated 1:1 orthologous genes.

Results and Discussion:

The total immune gene transcriptional response to LPS scaled hypermetrically. Baseline expression of the sum of all transcripts from one-to-one orthologous genes with immune annotations did not scale significantly differently from isometry ($-0.18 < \beta_2 \sim -0.04 < 0.10$), but the transcriptional response to LPS of the same genes did scale hypermetrically with 95% credibility ($0.02 < \beta_3 \sim 0.14 < 0.26$, Figs. 3, S1). Although the total expression of immune genes after LPS exposure did not scale with significant allometry ($-0.04 < \beta_2 + \beta_3 \sim 0.10 < 0.24$), the estimate was also large and positive, allowing for the possibility that larger primates have disproportionally higher concentrations of immune gene transcripts during sepsis than do smaller primates. The sum of all reads from genes that belong to immune-annotated orthogroups (allowing for apparent duplications and deletions) also had hypermetric estimates for both response to LPS and total expression during sepsis, although these were not 95% credible ($-0.02 < \beta_3 \sim 0.12 < 0.25$; $-0.07 < \beta_2 + \beta_3 \sim 0.11 < 0.29$, Figs. S2-3).

Individual immune-annotated genes are more likely than non-immune genes to scale hypermetrically. Although the total expression of immune-annotated genes is an important measure of the total activity of cells, it is possible that such a pattern is driven by the expression of a small number of highly-expressed genes. Thus, to assess broader trends across the transcriptome, we additionally analyzed the expression of each one-to-one orthologous gene in our dataset and classified them as hypometric, isometric, or hypermetric. Using Fisher's exact tests on the resulting contingency tables, we found that individual immune-annotated genes are more likely than non-immune-annotated genes to have hypermetric scaling of their LPS response ($P < 0.0001$) and expression after LPS ($P < 0.0001$), but not their baseline expression ($P = 0.76$) (Table 1; Data S2).

Allometry	Quantity	Immune genes	Non-immune genes	P-value (Fisher)
hypermetric	LPS(-)	53 (12%)	495 (13%)	0.7616
isometric	LPS(-)	333 (78%)	2971 (78%)	0.8537
hypometric	LPS(-)	43 (10%)	341 (9%)	0.4776
hypermetric	Δ-LPS	66 (15%)	343 (9%)	**0.0001**
isometric	Δ-LPS	334 (78%)	3076 (80%)	0.1571
hypometric	Δ-LPS	29 (7%)	388 (10%)	**0.0258**
hypermetric	LPS(+)	65 (15%)	245 (6%)	**< 0.0001**
isometric	LPS(+)	334 (78%)	3289 (86%)	**< 0.0001**
hypometric	LPS(+)	30 (7%)	273 (7%)	1.0000

Table 1. Number of immune- or non-immune-annotated genes with hypometric, hypermetric, or approximately isometric scaling. Innate immune annotations were derived from Deschamps *et al*. 2016. Genes were considered hypometric for a given quantity if the pGLMM 95% credible interval for the corresponding beta was entirely negative, hypermetric if it was entirely positive, and isometric if it included zero. P-values correspond to Fisher's exact test comparing the proportions of immune or non-immune genes with each allometric pattern vs the sum of the other two patterns.

Exaggerated LPS response in larger animals supports Safety Factor dynamics. Our results show that immune gene expression is indeed associated with body mass in a disproportionate (i.e., allometric) manner. Large primates increase their immune gene expression more during simulated sepsis than small primates, which may result in disproportionately greater concentrations of immune-related gene transcripts during infection in large species (Fig. 3). This result suggests that immune defense genes have greater priority in larger animals relative to other genes, consistent with the Safety Factor hypothesis.

Notably, genes with hypermetric responses and concentrations are represented by diverse immune functions, such as pathogen and damage sensors, transcription factors, and effectors (Data S2). This result underlines the fact that the allometry of immune gene transcription is quite general. However, the mechanisms of regulation still warrant further investigation. We note that not all immune-annotated genes result in greater defense capabilities when expressed more; for example, the gene *CTLA4* is known to be a *negative* regulator of inflammation and immune response (*25*). Its hypermetric baseline expression might mitigate runaway positive feedback loops which could otherwise result from the hypermetric expression of other, positive, regulators. The allometry of this gene was also notable because the direction of LPS response appears to reverse across the range of primate body sizes: in the smallest species, LPS exposure resulted in increased expression, while in the largest species, LPS exposure resulted in decreased expression. This pattern could have important implications for the interpretation of studies that use model organisms to draw conclusions about this gene in humans.

Eco-evolutionary implications of our results. Allometry in the magnitude of infection response may affect pathogen and parasite evolution (*16*). If smaller organisms tend to have less aggressive immune responses to a given stimulus than larger organisms, then pathogens that evolve to infect smaller organisms may have less selective pressure to minimize the stimulus that they produce. Thus, pathogens are likely to be generally more successful at jumping from large species to small species than the reverse. However, the occasional pathogen that does successfully jump from a small species to a large speces may be more likely to cause immunopathologies in their new host. For example, cytokine storms contribute significantly to COVID-19 severity in humans, with the immune system's extreme response potentially causing at least as much harm as direct damage from SARS-CoV-2 (*26*, *27*). This perspective may at first appear to conflict with the idea of a protective 'Safety Factor' in larger animals. However, this trend could be the result of complex trade-offs between the increased probability of localized self-harm and a reduced probability for systemic damage to a large-bodied individual. More aggressive immune responses are likely to help contain infections to smaller areas of the body. Further investigation into these possibilities could help inform predictions about the severity and pathology of future zoonotic events and provide valuable insights into the complex relationship between body size and immunity.

Materials and Methods:

***Sample collection*.** We collaborated with San Antonio Primate Center, the Duke Lemur Center, the Sedgwick County Zoo and the USF Health Clinic to obtain fresh whole blood samples from nine primate species, including humans, spanning more than three orders of magnitude of body mass, ranging from a 64 g *Microcebus murinus* to a 124,100 g *Pongo abelii*. Our final dataset included two aye-ayes (*Daubentonia madagascariensis*), four ring-tailed lemurs (*Lemur catta*), four tufted capuchins (*Sapajus apella*), four Rhesus macaques (*Macaca mulatta*), two olive baboons (*Papio anubis*), two hybrid olive/yellow baboons (*Papio anubis cynocephalus*, treated as *P. anubis* for all analyses), four (4) common marmosets (*Callithrix jacchus*), eight mouse lemurs (in a single pooled sample; *M. murinus*), one human (*Homo sapiens*), and one Sumatran orangutan (*P. abelii*). We focused sampling on males to minimize sex differences in gene expression. (Fig. 2, Dataset S1).

A fresh, venous whole blood sample (2 mL) was collected from each individual animal by collaborators and the date and time were noted. One milliliter of fresh blood was then transferred to each of two TruCulture tubes (Myriad RBM) containing 2 mL of a proprietary media mixture (1-part blood to 2-parts media). One tube (LPS treatment) contained 1 μg/mL of 055:B5 strain LPS (782-001087) and the other (null treatment) contained only the growth media (782-001086). Each tube was then inverted three times to ensure adequate mixing and incubated at 37 °C for 8 hours. We chose 8 hours to balance the initial burst of pro-inflammatory cytokines, which peak in humans 4 hours after an LPS challenge, and the later increase of other cytokines such as IL8, which peaks at 24 hours (*28*). After incubation, tubes were centrifuged at 400-500 g for 10 min. The seraplas filter was then inserted into the tube and the supernatant (plasma/media layer) was removed. The cells left at the bottom of the tube were then transferred to a new 2 mL cryovial, RNAlater (Qiagen) was added and frozen at -80°C until RNA extraction could be completed. In the case where a 2 mL blood draw was not possible (only for 1 marmoset and 1 capuchin), the ratios inside the TruCulture tube were adjusted so that the 1:2 blood:media was consistent across samples. Because of the small body mass of the mouse lemurs, we pooled blood from eight individuals and distributed that 2 mL blood pool equally across the two samples (null and LPS).

De-identified blood samples were collected on human samples. All studies performed on human subjects were performed in accordance with Institutional Review Board Approved Protocols as well as guidelines in the 1964 Declaration of Helsinki and its later amendments, with written informed consent obtained from patients.

***Whole blood RNA extraction*.** We used a Trizol-based protocol to extract RNA from primate samples using the Direct-zol RNA Microprep kit (R2060, Zymo Research). All steps were centrifuged at 13,000 g for 30 s unless otherwise noted. Briefly, 9 μl Proteinase K was added to a 300 μl sample stored in RNAlater and incubated for 30 min. Then, 2.0 mL Trizol was added to

the sample and incubated while vortexing for 15 min. We then added 2.3 mL ethanol to the mixture and vortexed it. The sample was added to a Zymo-spin IC Column fitted with a collection tube in 700 µl increments (the maximum loading volume of the column). After each increment, the sample was centrifuged, and the flow-through discarded. We then performed the DNase treatment steps. We added 400 µl RNA wash buffer and centrifuged the sample, and then added 5 µl DNAse 1 and 35 µl DNA digestion buffer and incubated it for 15 min. We added 400 µl Direct-zol RNA prewash buffer to the column, centrifuged and discarded flow-through (x2). Then 700 µl of RNA wash buffer was added to the column and centrifuged for 1.5 min to ensure removal of buffers. Finally, 10 µl of RNase-free water was then added directly to the column matrix, incubated for 1 min, and centrifuged. Concentrations and quality of each sample were checked via RNA broad range Qubit fluorometric quantification (Q10210, Thermo Fisher Scientific) and Agilent tape station 2200 (Agilent), respectively.

***Library preparation and RNAseq*.** Extracted RNA samples were submitted to the University of Illinois at Urbana-Champaign Roy J. Carver Biotechnology Center for library preparation. Libraries were prepared with the Ovation SOLO RNAseq kit (M01406, Tecan) with probes for human rRNA and globin RNA. They were sequenced with the NovaSeq 6000 with an S4 flow-cell and 150 bp paired-end reads.

***Reference transcriptomes, orthogroups, and gene expression quantification*.** ENSEMBL (release 109) (*29*) reference transcriptomes (*.cdna.all.fa.gz) were used for *M. murinus*, *C. jacchus*, *P. anubis*, *M. mulatta*, *P. abelii*, and *H. sapiens*. Because *L. catta*, *D. madagascariensis*, and *S. apella* are not yet integrated into ENSEMBL, reference transcriptomes were created with the following workflow. First, NCBI GenBank genomes were acquired (GCF_020740605.2, GCA_023783475.1, and GCF_009761245.1, respectively), and HISAT2 v2.1.0 (*30*) indexes were built. Then, sequencing reads for each sample were assembled into 'superreads' using the superreads.pl script provided for use with StringTie v1 (*31*). Superreads and unassembled paired-end reads were then mapped to their respective genome using HISAT2 with options --no-discordant --no-mixed --dta-cufflinks. StringTie v2.2.1(*32*) was then used to generate transcriptomes with default settings. TransDecoder v5.5.0 (*33*) was used to predict peptide sequences. The longest predicted peptide was isolated for each gene, and these peptides were input to Orthofinder v2.5.4 (*34*) in combination with ENSEMBL reference peptides (filtered from Compara.109.protein_default.aa.fasta.gz) to identify orthogroups across all nine species. The phylogeny from Hedges *et al.* 2015 was subsetted and used as a fixed species tree in the Orthofinder analysis. Gene expression estimates were generated using Salmon v1.6.0 (*35*) with default settings and raw sequencing reads from each sample.

***Differential abundance analysis of genes*.** To assess differential abundance of each gene, count data were analyzed with phylogenetic generalized linear mixed models using the function pglmm() from the R package *phyr* v1.1.0 (*36*). To approximately account for the discrete and

compositional nature of RNASeq count data, a Poisson likelihood with a log link was used with an offset term unique to each observation. This offset was determined by importing Salmon quantification outputs into an R object with the package *tximport* v1.26.1 (*37*), filtering the genes to include only 1:1 orthologs as previously determined with Orthofinder, and using the DESeq2 v1.38.2 (*38*) function *estimateSizeFactors*. The resulting 'normalization factors' are designed to compensate for varying sequencing depth, compositionality, and average transcript length across samples. Binary LPS treatment, the standardized log of each species' average body mass (*24*), the standardized log of species-normalized individual body size, and the interaction of LPS treatment with each body size effect, were modeled as fixed effects (β_1-β_5), with random effects for individual, independent and identically distributed (i.i.d.) species, species phylogeny, and the interactions between the treatment and i.i.d. species and species phylogeny. *phyr* also automatically includes an observation-level random effect to account for overdispersion relative to the expected variance of the Poisson likelihood. The afore-mentioned phylogenetic tree from Hedges *et al.* 2015 (*23*) was used for phylogenetic random effects. In this model, the main effect of LPS treatment (β_1) can be interpreted as the change in expression after LPS treatment for each gene at the ancestral body size (somewhat arbitrary for the purposes of this study, and determined by optimization with the *ace* function from the R package *ape* 5.7-1 (*39*)), the main effect of species' average body mass (β_2) can be interpreted as the allometric effect on the baseline expression of each gene, the interaction between LPS treatment and species' average body mass (β_3) can be interpreted as the allometric effect on change in expression after LPS treatment, the main effect of species-normalized individual body size (β_4) may be caused by either aging-related changes or within-species allometric differences in the baseline expression of each gene, and the interaction between LPS treatment and species-normalized individual body size (β_5) may be caused by either aging-related changes or within-species allometric differences in the change in expression after LPS treatment. The random effect for individuals enables the model to focus on paired differences between and LPS and null treatment, the main species effects control for incidentally correlated evolution of body mass and baseline gene expression, and the species interaction effects control for incidentally correlated evolution of body mass and the change in expression during LPS treatment. The model was fit using approximate Bayesian inference with default priors with *INLA* v21.02.23 (*40*). The sums of β_2 and β_3 and of β_4 and β_5 were calculated during model fitting using *INLA*'s 'lincomb' option, to represent the actual allometric slopes among LPS-treated samples. Fixed effect coefficients were extracted, and individual genes were determined to have significant differential relative abundance if their 95% credible interval did not contain zero. Two-by-two contingency tables were constructed summarizing the number of genes that were allometric (or not) and immune-annotate (or not), and Fisher's exact tests were used to determine if each allometric pattern was more likely in immune vs. non-immune genes.

***Differential abundance analysis of total immune genes*.** Orthologous gene sets were annotated with their corresponding immune functions as defined by Deschamps *et al*. 2016 (*41*). External

gene names were determined for each ortholog by querying the Ensembl BioMart (*29*) with the R package *biomaRt* v2.54.1 (*42*), using human members of each orthogroup, and these gene names were used to extract immune function annotations from Table S1 from Deschamps *et al*. Two workflows were used to assess the total expression of immune genes. In the first, counts for all immune-annotated 1:1 orthologs were summed, and average gene lengths for the pool were calculated for use in DESeq2's normalization factor calculations. This method is conservative in focusing only on identifiable 1:1 orthologs, and can utilize observation-specific normalization factors so that results may be interpreted as differences in the number of transcripts across samples. In the second, counts of all genes that belonged to immune-annotated orthogroups were pooled, and 'size factors' that were consistent for a given sample were calculated by taking the geometric mean of the normalization factors of all 1:1 orthologs. This method is more comprehensive, covering all genes with likely immune functions, but because it does not compensate for differences in average transcript length across samples, it is *less confidently* interpretable as differences in numbers of transcripts. The choice to use 'size factors' instead of 'normalization factors' here was made because it is likely that gene predictions are fragmented for the three species with lower-quality references, and apparent gene duplications or losses in these species could artificially influence the predicted average transcript length. However, by focusing directly on the number of reads rather than on the inferred number of transcripts, this version may actually represent a more direct measure of the amount of energy expended during transcription. For both analyses, total immune gene abundance was modeled with *phyr* and *INLA* using the same protocol and formula as analyses of individual genes.

All analyses that used R throughout the manuscript used version 4.2.2 (*43*). The packages *ggtree* v3.6.2 (*44*) and *ggplot2* v3.4.1 (*45*) were used for plotting.

Acknowledgements: The authors thank Debbie Christian, Deborah Chavez, and Chris Chen at the Southwest National Primate Research Center at the Texas Biomedical Research Institute; Erin Ehmke, Kay Welser, and Megan Davison at the Duke Lemur Center; Jennifer Kropf and Sandy Wilson at the Sedgwick County Zoo in their collaboration and support in obtaining and processing these primate samples. We thank Manfred Schmolz at Myriad RBM for help with TruCulture techniques and Alvaro Hernandez in troubleshooting RNA extractions and sequencing. Finally, thanks to Samantha Oakey, Matthew Mercurio, Min Zhang, and the University of South Florida Genomics Program Sequencing Core and Computational Core/Omics Hub for laboratory and computational support.

Funding:

National Science Foundation Division of Integrative Organismal Systems grant NSF-IOS 1656551 (CJD)

National Science Foundation Division of Integrative Organismal Systems grant NSF-IOS 1656618 (LBM)

Author contributions:

Conceptualization: CJD, LBM, RHYJ, RM
Data curation: RM, ECR, SRA, RAM
Formal analysis: RM
Funding acquisition: CJD, LBM
Investigation: ECR, SRA
Methodology: RM, ECR, SRA, CJD, LBM, RHYJ
Project administration: CJD, LBM
Resources: ECR, CJD, LBM, JWL
Supervision: CJD, LBM, RHYJ
Visualization: RM
Writing – original draft: RM, CJD, LBM
Writing – review & editing: RM, CJD, LBM, RHYJ, RAM, ECR, SRA, JWL

Competing interests: J.W.L. is an employee and shareholder of Bluebird Bio, a speaker, consultant, and research funding recipient of Horizon Therapeutics, a speaker and consultant for Sobi, and on the advisory board of ADMA.

Data and materials availability: Quality-trimmed RNASeq data is available in NCBI BioProject PRJNA834816. All code used for analysis is available at https://github.com/rmcminds/McMinds_et_al_2022 and at Zenodo (doi:10.5281/zenodo.7915971).

Supplementary Materials:

Figs. S1 to S3

Data S1 to S2

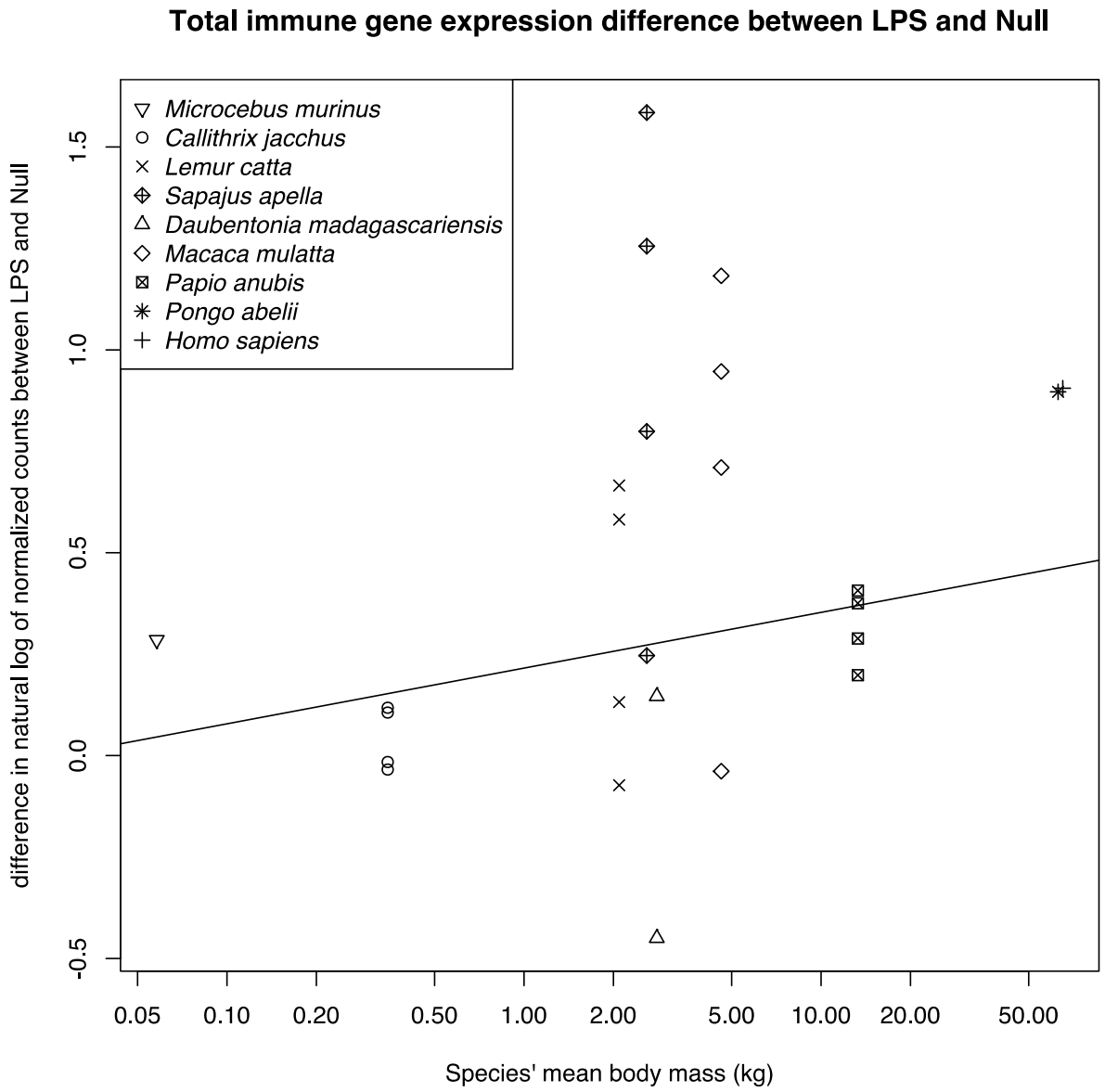

Fig. S1. Summed counts of all immune-annotated 1:1 orthologous genes show hypermetric response to sepsis. This figure draws on the same data as Figure 3 in the main text, but shows the difference between LPS- and Null-treated samples from each individual rather than the raw expression values.

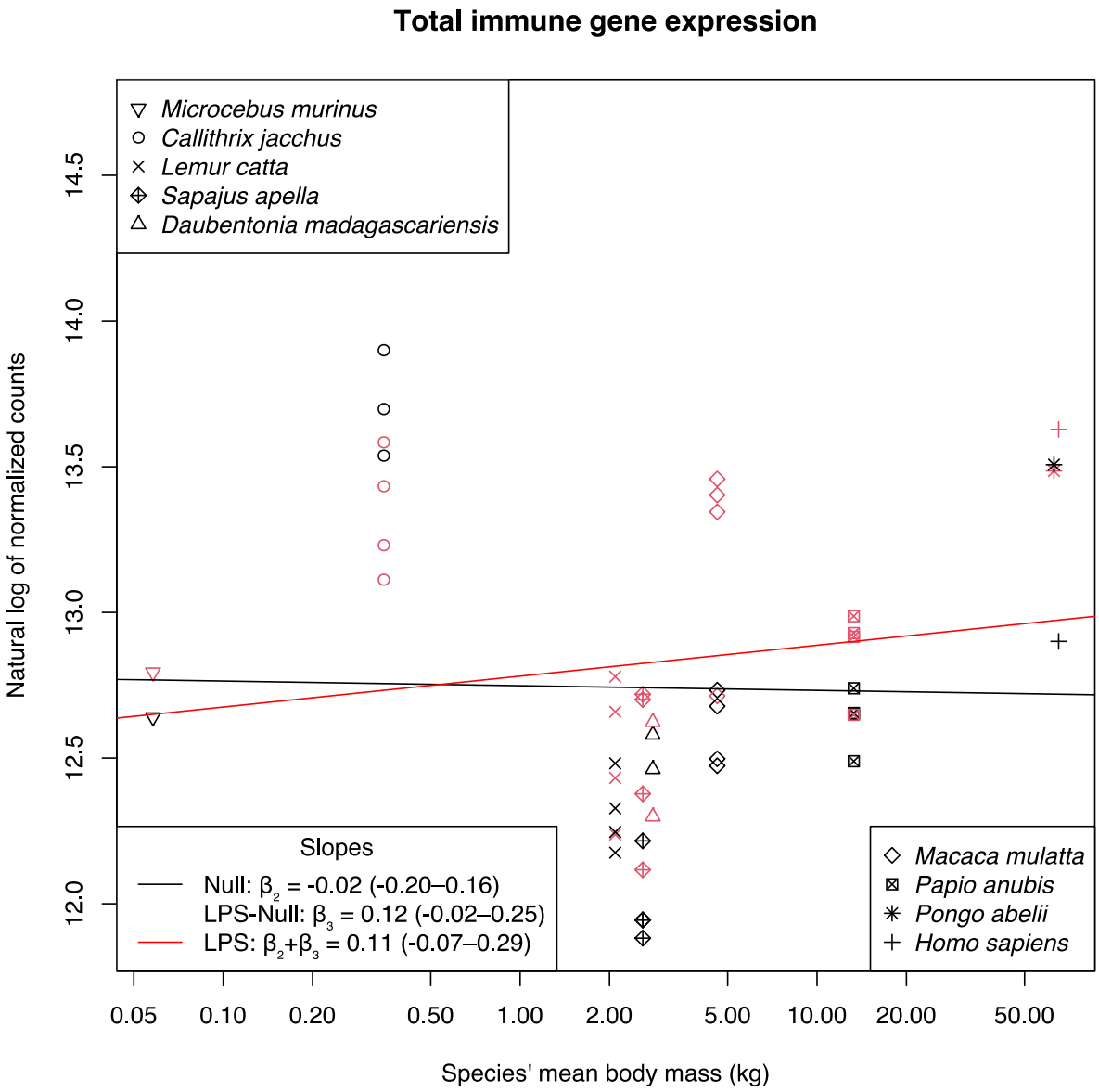

Fig S2. Summed counts of all immune-annotated reads show no significant allometry. This figure is analogous to Figure 3 in the main text, but is the sum of all reads annotated with immune functions, even if they belong to orthogroups that had duplications or gene deletions. This analysis is more comprehensive as it was able to include more genes (>1200 compared to >4000), but is probably more susceptible to differences in gene lengths, or apparent gene lengths due to lower quality transcriptome assemblies. As an alternate method with different assumptions that shows something similar, it's a nice backup. Theoretically, this might be better interpreted as an increase in total immune-related RNA, whereas the other is an increase in the total number of immune-annotated transcripts. This analysis might be more directly related to energy expenditure on transcription, whereas the analysis of only one-to-one orthologs might be more closely related to the number of molecules and potentially effectiveness of the response.

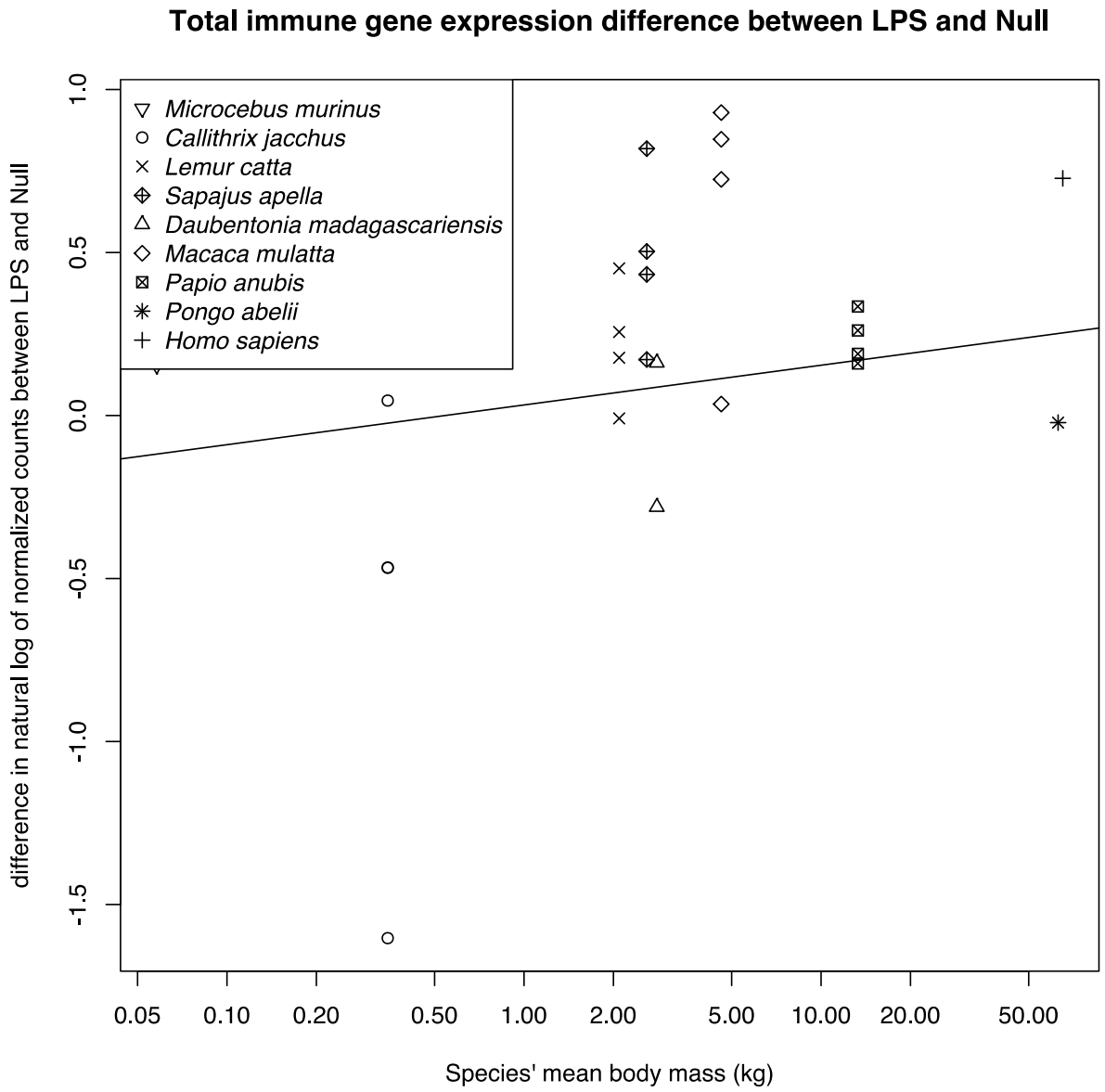

Fig. S3. Sum of all counts of reads that belong to immune-annotated orthogroups. This figure is the same as Figure S1, but including all immune reads rather than just 1:1 orthologs.

References

1. G. B. West, *Scale: the universal laws of growth, innovation, sustainability, and the pace of life in organisms, cities, economies, and companies* (2017).

2. V. M. Savage, J. F. Gillooly, W. H. Woodruff, G. B. West, A. P. Allen, B. J. Enquist, J. H. Brown, The predominance of quarter-power scaling in biology. *Funct Ecol*. 18, 257–282 (2004).

3. J. W. Prothero, *The design of mammals* (2015).

4. W. A. Calder, *Size, function, and life history* (Harvard University Press, 1996).

5. J. H. Brown, J. F. Gillooly, A. P. Allen, V. M. Savage, G. B. West, Toward a metabolic theory of ecology. *Ecology*. 85, 1771–1789 (2004).

6. H. A. Feldman, T. A. McMahon, The 3/4 mass exponent for energy metabolism is not a statistical artifact. *Resp Physiol*. 52, 149–163 (1983).

7. M. Kleiber, Body size and metabolism. *Hilgardia*. 6, 315–353 (1932).

8. G. B. West, J. H. Brown, B. J. Enquist, A general model for the origin of allometric scaling laws in biology. *Science*. 276, 122–126 (1997).

9. H. S. Horn, Commentary on Brown et al.'s "Toward a metabolic theory of ecology." *Ecology*. 85, 1816–1818 (2004).

10. M. P. O'Connor, S. J. Kemp, S. J. Agosta, F. Hansen, A. E. Sieg, B. P. Wallace, J. N. McNair, A. E. Dunham, Reconsidering the mechanistic basis of the metabolic theory of ecology. *Oikos*. 116, 1058–1072 (2007).

11. C. J. Downs, J. P. Hayes, C. R. Tracy, Scaling metabolic rate with body mass and inverse body temperature: a test of the Arrhenius fractal supply model. *Funct Ecol*. 22, 239–244 (2008).

12. D. S. Glazier, Is metabolic rate a universal 'pacemaker' for biological processes? *Biol Rev*. 90, 377–407 (2015).

13. D. Dingli, J. M. Pacheco, Allometric scaling of the active hematopoietic stem cell pool across mammals. *Plos One*. 1, e2 (2006).

14. E. C. Ruhs, L. B. Martin, C. J. Downs, The impacts of body mass on immune cell concentrations in birds. *Proc Royal Soc B Biological Sci*. 287, 20200655 (2020).

15. C. J. Downs, N. A. Dochtermann, R. Ball, K. C. Klasing, L. B. Martin, The effects of body mass on immune cell concentrations of mammals. *Am Nat*. 195, 107–114 (2020).

16. C. J. Downs, L. A. Schoenle, B. A. Han, J. F. Harrison, L. B. Martin, Scaling of host competence. *Trends Parasitol*. 35, 182–192 (2019).

17. M. L. D. Lopez, Y. Lin, S. Q. Schneider, C. Hsieh, F. Shiah, R. J. Machida, Allometric scaling of interspecific RNA transcript abundance to extend the use of metatranscriptomics in characterizing complex communities. *Mol Ecol Resour*. 23, 52–63 (2023).

18. M. B. F. Hawash, J. Sanz-Remón, J.-C. Grenier, J. Kohn, V. Yotova, Z. Johnson, R. E. Lanford, J. F. Brinkworth, L. B. Barreiro, Primate innate immune responses to bacterial and viral

pathogens reveals an evolutionary trade-off between strength and specificity. *Proc National Acad Sci*. 118, e2015855118 (2021).

19. C. Vaure, Y. Liu, A comparative review of Toll-like receptor 4 expression and functionality in different animal species. *Front Immunol*. 5, 316 (2014).

20. P. D. Coley, J. P. Bryant, F. S. C. III, Resource availability and plant antiherbivore defense. *Science*. 230, 895–899 (1985).

21. L. B. Martin, Z. M. Weil, R. J. Nelson, Immune defense and reproductive pace of life in Peromyscus mice. *Ecology*. 88, 2516–2528 (2007).

22. L. B. Martin, Z. M. Weil, R. J. Nelson, Fever and sickness behaviour vary among congeneric rodents. *Funct Ecol*. 22, 68–77 (2008).

23. S. B. Hedges, J. Marin, M. Suleski, M. Paymer, S. Kumar, Tree of Life Reveals Clock-Like Speciation and Diversification. *Mol Biol Evol*. 32, 835–845 (2015).

24. J. R. Burger, M. A. George, C. Leadbetter, F. Shaikh, The allometry of brain size in mammals. *J Mammal*. 100, 276–283 (2019).

25. T. Nakajima, C. J. Suarez, K.-W. Lin, K. Y. Jen, J. E. Schnitzer, S. S. Makani, N. Parker, D. L. Perkins, P. W. Finn, T Cell Pathways Involving CTLA4 Contribute To a Model of Acute Lung Injury. *J Immunol*. 184, 5835–5841 (2010).

26. B. Hu, S. Huang, L. Yin, The cytokine storm and COVID-19. *J Med Virol*. 93, 250–256 (2021).

27. M. H. Lee, D. P. Perl, J. Steiner, N. Pasternack, W. Li, D. Maric, F. Safavi, I. Horkayne-Szakaly, R. Jones, M. N. Stram, J. T. Moncur, M. Hefti, R. D. Folkerth, A. Nath, Neurovascular injury with complement activation and inflammation in COVID-19. *Brain*. 145, awac151 (2022).

28. L. E. DeForge, D. G. Remick, Kinetics of TNF, IL-6, and IL-8 gene expression in LPS-stimulated human whole blood. *Biochem Bioph Res Co*. 174, 18–24 (1991).

29. F. Cunningham, J. E. Allen, J. Allen, J. Alvarez-Jarreta, M. R. Amode, I. M. Armean, O. Austine-Orimoloye, A. G. Azov, I. Barnes, R. Bennett, A. Berry, J. Bhai, A. Bignell, K. Billis, S. Boddu, L. Brooks, M. Charkhchi, C. Cummins, L. Da Rin Fioretto, C. Davidson, K. Dodiya, S. Donaldson, B. El Houdaigui, T. El Naboulsi, R. Fatima, C. G. Giron, T. Genez, J. G. Martinez, C. Guijarro-Clarke, A. Gymer, M. Hardy, Z. Hollis, T. Hourlier, T. Hunt, T. Juettemann, V. Kaikala, M. Kay, I. Lavidas, T. Le, D. Lemos, J. C. Marugán, S. Mohanan, A. Mushtaq, M. Naven, D. N. Ogeh, A. Parker, A. Parton, M. Perry, I. Piližota, I. Prosovetskaia, M. P. Sakthivel, A. I. A. Salam, B. M. Schmitt, H. Schuilenburg, D. Sheppard, J. G. Pérez-Silva, W. Stark, E. Steed, K. Sutinen, R. Sukumaran, D. Sumathipala, M.-M. Suner, M. Szpak, A. Thormann, F. F. Tricomi, D. Urbina-Gómez, A. Veidenberg, T. A. Walsh, B. Walts, N. Willhoft, A. Winterbottom, E. Wass, M. Chakiachvili, B. Flint, A. Frankish, S. Giorgetti, L. Haggerty, S. E.

Hunt, G. R. IIsley, J. E. Loveland, F. J. Martin, B. Moore, J. M. Mudge, M. Muffato, E. Perry, M. Ruffier, J. Tate, D. Thybert, S. J. Trevanion, S. Dyer, P. W. Harrison, K. L. Howe, A. D. Yates, D. R. Zerbino, P. Flicek, Ensembl 2022. *Nucleic Acids Res*. 50, D988–D995 (2021).

30. D. Kim, J. M. Paggi, C. Park, C. Bennett, S. L. Salzberg, Graph-based genome alignment and genotyping with HISAT2 and HISAT-genotype. *Nat Biotechnol*. 37, 907–915 (2019).

31. M. Pertea, G. M. Pertea, C. M. Antonescu, T.-C. Chang, J. T. Mendell, S. L. Salzberg, StringTie enables improved reconstruction of a transcriptome from RNA-seq reads. *Nat Biotechnol*. 33, 290–295 (2015).

32. S. Kovaka, A. V. Zimin, G. M. Pertea, R. Razaghi, S. L. Salzberg, M. Pertea, Transcriptome assembly from long-read RNA-seq alignments with StringTie2. *Genome Biol*. 20, 278 (2019).

33. B. Haas, *TransDecoder* (2022).

34. D. M. Emms, S. Kelly, OrthoFinder: phylogenetic orthology inference for comparative genomics. *Genome Biol*. 20, 238 (2019).

35. R. Patro, G. Duggal, M. I. Love, R. A. Irizarry, C. Kingsford, Salmon provides fast and bias-aware quantification of transcript expression. *Nat Methods*. 14, 417–419 (2017).

36. D. Li, R. Dinnage, L. A. Nell, M. R. Helmus, A. R. Ives, phyr: An r package for phylogenetic species-distribution modelling in ecological communities. *Methods Ecol Evol*. 11, 1455–1463 (2020).

37. C. Soneson, M. I. Love, M. D. Robinson, Differential analyses for RNA-seq: transcript-level estimates improve gene-level inferences. *F1000research*. 4, 1521 (2016).

38. M. I. Love, W. Huber, S. Anders, Moderated estimation of fold change and dispersion for RNA-seq data with DESeq2. *Genome Biology*. 15 (2014), doi:10.1186/s13059-014-0550-8.

39. E. Paradis, J. Claude, K. Strimmer, APE: Analyses of Phylogenetics and Evolution in R language. *Bioinformatics*. 20, 289–290 (2004).

40. H. Rue, A. Riebler, S. H. Sørbye, J. B. Illian, D. P. Simpson, F. K. Lindgren, Bayesian computing with INLA: a review. *Arxiv* (2016).

41. M. Deschamps, G. Laval, M. Fagny, Y. Itan, L. Abel, J.-L. Casanova, E. Patin, L. Quintana-Murci, Genomic signatures of selective pressures and introgression from archaic hominins at human innate immunity genes. *Am J Hum Genetics*. 98, 5–21 (2016).

42. S. Durinck, Y. Moreau, A. Kasprzyk, S. Davis, B. D. Moor, A. Brazma, W. Huber, BioMart and Bioconductor: a powerful link between biological databases and microarray data analysis. *Bioinformatics*. 21, 3439–3440 (2005).

43. R. C. Team, *R: a language and environment for statistical computing* (R Foundation for Statistical Computing, Vienna, Austria, 2021; https://www.R-project.org/).

44. G. Yu, D. K. Smith, H. Zhu, Y. Guan, T. T. Lam, ggtree: an R package for visualization and annotation of phylogenetic trees with their covariates and other associated data. *Methods Ecol Evol*. 8, 28–36 (2017).

45. H. Wickham, *ggplot2: Elegant Graphics for Data Analysis* (Springer-Verlag New York, 2016; https://ggplot2.tidyverse.org).